Surface & Coatings Technology 309 (2017) 423–435

Contents lists available at ScienceDirect

Surface & Coatings Technology

journal homepage: www.elsevier.com/locate/surfcoat

# The effect of pure aluminum cold spray coating on corrosion and corrosion fatigue of magnesium (3% Al-1% Zn) extrusion

Mohammad Diab [a], Xin Pang [b], Hamid Jahed [a,*]

[a] Mechanical and Mechatronics Engineering Department, University of Waterloo, 200 University Avenue West, Waterloo, ON N2L 3G1, Canada
[b] CanmetMATERIALS, Natural Resources Canada, 183 Longwood Road South, Hamilton, ON L8P 0A5, Canada

ARTICLE INFO

*Article history:*
Received 2 July 2016
Revised 13 October 2016
Accepted in revised form 5 November 2016
Available online 11 November 2016

*Keywords:*
Cold spray
Pure aluminum
AZ31B extrusion
Corrosion
Corrosion fatigue

ABSTRACT

Pure aluminum powder was successfully sprayed on AZ31B extrusion flat and round coupons at low temperature. The corrosion and corrosion fatigue behavior of the coated and uncoated samples were examined by performing accelerated corrosion tests. The corrosion resistance of AZ31B samples with and without coating was investigated based on ASTM B117 standard salt spray with a concentration of 5% NaCl at 36 °C, 100% relative humidity. The corrosion fatigue of bare and coated round samples was examined by producing a thin film of 3.5% NaCl solution on the surface of the fatigue samples via integrating a corrosion chamber into a rotating bending fatigue testing machine. Pure Al coating provided significant corrosion protection for AZ31B in 5% NaCl fog environment by improving its corrosion resistance from 90% average weight loss in 33 days for bare samples to <10% average weight loss in 90 days of continuous corrosion cycles. However, pure Al coating did not improve the corrosion fatigue strength of magnesium and samples with and without coating showed similar corrosion fatigue trends. Test results in salt solution showed fatigue life reduction of 88% when compared with test results in air. The microstructure examination of samples failed under cyclic load showed early cracking of Al coat which allowed the electrolyte penetration into Mg substrate creating a localized corrosion and premature failure. The early cracking was attributed to the lower fatigue strength of pure Al compared to AZ31B.


## 1. Introduction

The low density of magnesium (Mg) and its alloys (1.74 g/cm$^{-3}$) which is two thirds of aluminum (Al) and one-fourth of steel densities [1], as well as their excellent specific strength, and machinability properties make them attractive candidates for structural lightweighting applications. The most prolific users of Mg are transportation industries like automotive and aerospace in which structural weight reduction is at the forefront of their design innovations. Magnesium, however, is one of the most electrochemically reactive materials and is therefore susceptible to corrosion in humid and aqueous environments. For this reason, the applications for Mg and its alloys have been limited [2–6]. The main benefit of Mg is its application toward load bearing components of transportation vehicles and therefore the protection of Mg from corrosion is essential. The loading on such components is cyclic in nature and hence corrosion fatigue behavior is a key factor in their design and application. In recent years, many researchers have studied the influencing factors in Mg corrosion [4,5,7–10].

Song et al. [7] and Holly [8] have shown that the chemical composition of α-phase and the presence of β-phase in Mg alloys are major factors in its corrosion behavior. The presence of the second phase particles in the microstructure of Mg-Al alloys can have two effects on the corrosion behavior of the alloy depending on the volume fraction and the distribution of the second phases [7]. The second phase particles can act either as a barrier or as a galvanic cathode to which the α-Mg is the galvanic anode. AZ91 alloy, for example, contains a large volume of β-phase ($Mg_{17}Al_{12}$) precipitates due to the high Al content, forming a network. In NaCl environment, the network of β-phase particles can work as a barrier and inhibit the corrosion of the AZ91 alloy surface [7]. On the other hand, the secondary phases and the grain boundaries, when dispersed, can also act as galvanic cathodes to the α-Mg matrix. If the α-Mg grain size is large, the second phase in the Mg alloy is agglomerated, and the distance between the second phase particles is large (for example in AZ31), then the presence of the second phase would increase the corrosion rate of the alloy [7–8]. For the wrought alloys, it has also been shown that twins and extrusion ratio can affect the corrosion behavior of Mg. The existence of twins increases the corrosion severity of the alloy and their elimination by heat treatments improved the corrosion resistance of the alloy [9]. The extrusion ratio of AZ31B was also studied and it was found that raising the extrusion ratio

* Corresponding author.
*E-mail address:* hjahedmo@uwaterloo.ca (H. Jahed).

http://dx.doi.org/10.1016/j.surfcoat.2016.11.014

resulted in a decrease in the grain size, which improved the corrosion resistance and enhanced the passivity of the alloy [5,10].

Among the protection methods and techniques available [11–14], Al powder cold spray is a rather new coating technology, which is a low temperature process that has shown promising results in corrosion protection [15]. Considerable research [16–20] has been conducted on coating Mg alloys with Al powder using cold spray technique and its effect on the corrosion resistance and mechanical properties of the alloys. Irissou et al. [16], Spencer et al. [17], and Tao et al. [18–19] studied the effect of pure Al and Al–$Al_2O_3$ mixed powder cold spray coating on Mg substrate. In comparison with pure Al powder, it was reported that Al-$Al_2O_3$ composite coating was stronger and exhibited better adhesion than the pure Al coating. Although the corrosion resistance of the pure Al and the Al-$Al_2O_3$ composite coatings was found to be similar, they both showed better corrosion resistance than bulk Al alloy [16–19]. It was also reported that using high purity Al powder ≥ 99.95 wt.% resulted in the highest adhesion strength and better corrosion performance, but on the other hand the coating had low hardness [15]. Hengyong et al. [20] reported that mixing hard ceramic intermetallic particles $Mg_{17}Al_{12}$ with pure Al powder with proper mix ratio significantly improved the bonding strength with no porosity as compared to the pure Al coating [20]. They also showed that the corrosion current densities and corrosion potentials of composite coatings were close to those of pure Al.

The corrosion of cold sprayed Mg alloy samples subjected to cyclic loads, however, has not received much attention. The corrosion fatigue properties of Mg are considered to be of both practical interest and fundamental importance [21]. The corrosion and corrosion fatigue of AZ31B extrusion with and without Al cold spray coating are investigated and discussed in this paper.

## 2. Materials and experiments

The material investigated in this study was Mg alloy AZ31B extrusion. Test samples were machined from an air-quenched AZ31B extrusion section (Fig. 1) manufactured by Timminco. The section was extruded from a 177.8 mm diameter, 406.4 mm long billet, with an extrusion ratio of 6. The extrusion temperature was between 360 and 382 °C, with an extrusion exit speed of 50.8 mm/s. The chemical composition and the mechanical properties of this alloy are given in Tables 1 and 2, respectively.

Flat coupons with dimensions of 260 mm × 75 mm × 1.5 mm were first wire cut from the extrusion piece. Half of the samples were cold spray coated with commercially available pure aluminum powder. The Al powder used was series SST-A05011 (Centerline Ltd., Windsor, Canada), with nominal purity of 99.93%, and density of 0.9–1.0 g/$cm^3$. The morphology of powder is shown in Fig. 2. As it can be seen from this figure the particles had irregular shape and their average particle size was measured to be 20 μm.

**Table 1**
Chemical composition of the extruded AZ31B (wt.%) [22].

| Al | Zn | Mn | Fe | Ni | Cu | Mg |
|---|---|---|---|---|---|---|
| 3.10 | 1.05 | 0.54 | 0.0035 | 0.0007 | 0.0008 | Bal. |

### 2.1. Cold spray coating

The cold spray coating was carried out at the Supersonic Spray Technologies (SST), Centerline Ltd. facilities in Windsor, Ontario. The sample surfaces were first degreased by acetone and then grit-blasted with aluminum oxide SST-G002 $Al_2O_3$ before the cold spray. Nitrogen (oxygen-free) gas was used as the carrier gas to accelerate the Al particles through a converging–diverging DeLaval nozzle to supersonic velocities in the high-pressure cold spray equipment. Samples were cold sprayed at gas temperature of 500 °C, with a gas pressure of 500 psi, step-over of 1.2 mm, standoff distance of 12 mm, gun speed of 120 mm/s, and powder feed-rate of 18–20 g/min. Flat samples were coated on large plates and then cut into coupons with dimensions of 50 mm × 75 mm × 1.5 mm for corrosion testing. The cold spray coating on the large plates ensured uniformity of coating across all coupons. A total of 27 bare and 20 coated samples were used for the corrosion testing (Fig. 3).

The coating and powder microstructure were examined using an Olympus BH61 optical microscope, Scanning Electron Microscope (SEM) and Energy Dispersive X-ray (EDX). Vickers hardness testing was performed on mounted and polished cross section samples from the coated coupons to measure the hardness profile for the Al coating, interface and Mg substrate. The tests were conducted according to ASTM E384-99 at room temperature with a 100 g indentation load and a 15 s holding time.

Fifty cylindrical specimens of AZ31B with dimensions shown in Fig. 4 were machined in the extrusion direction and prepared for the corrosion fatigue tests. The gauge sections of one half of the samples were cold sprayed by Al using the same parameters used for flat samples. Coating on round samples was performed with samples mounted on a rotating chuck and gun traveling across the gauge.

In an earlier work [23] and using XRD measurements it was found that an initial residual stress existed in the as-received extrusion pieces. This stress was due to the hot extrusion process and the different cooling rates across the extrusion piece. To ensure similar initial state for fatigue samples, all cylindrical specimens were stress relieved at 260 °C for 15 min, as per the ASM stress relieve process [24], in order to eliminate any internal residual stresses that may have accumulated in the hot extrusion process. Heat treatments were performed at Bodycote Thermal Processing, Kitchener, Ontario, Canada. The stress relief process was performed prior to cold spray coating and after cutting and machining round samples.

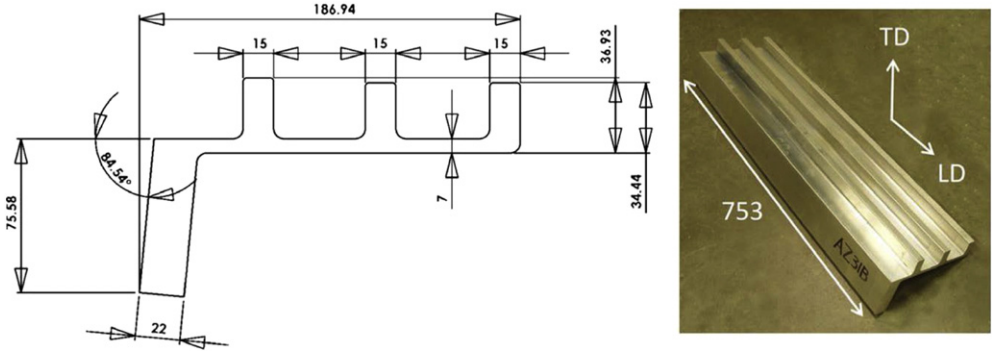


**Fig. 1.** Dimensions of the AZ31B extrusion (all dimensions in mm) [22], corrosion and corrosion fatigue samples machined from 7 mm thick and 15 mm thick sections, respectively.

**Table 2**
Mechanical properties of the material in extrusion direction [22].

| Crystal structure | Elastic modulus (GPa) | Ultimate tensile strength (MPa) | Ultimate compressive strength (MPa) | Yield strength in tension (MPa) | Yield strength in compression (MPa) |
|---|---|---|---|---|---|
| HCP | 44.8 | 227 | 364 | 213 | 108 |

### 2.2. Corrosion tests

The corrosion tests on coated and un-coated flat samples were performed according to ASTM B117 standard [25]. The testing coupons were exposed to a static environment of continuous salt spray with a concentration of 5% NaCl at 36 °C, 100% relative humidity. The Singleton Corp. SCCH - Salt Fog Chamber (Fig. 5) used for this study contains atomizing nozzles to atomize the salt solution within the chamber, a salt solution reservoir, specimen supports angled at 15° to 20° from the vertical direction, heating elements and controllers, and a humidifying tower connected to the reservoir. The temperature in the chamber was maintained between 36 and 37 °C during the test while the temperature in the humidifying tower was maintained at 47 °C. The salt solution container had a capacity of 60 l and was regularly filled with fresh 5% NaCl with a pH between 6.5 and 7.2. A pH meter was used to measure the prepared solution pH and buffer solutions were used for calibrating the pH meter before any use. Addition of acid (10% hydrochloric acid) or base (sodium hydroxide) was necessary from time to time in order to adjust the pH of the salt solution to be within the recommended value. The fog in the chamber was collected with a fog collector in the vicinity of the specimens periodically to ensure that the fog quantity is within the range of 1.0–2.0 ml per hour per 80 $cm^2$ as per ASTM B117 standard. The specimens were subjected to a continuous dense saline fog. Due to low thickness of the coupons the edges of samples were not sprayed. Miccrostop lacquer mask was used to mask off the exposed edges to prevent corrosion attack from the edges (Fig. 5b). Samples were taken from the chamber in different intervals, mainly after every three days of exposure. The last coated samples were taken out after 90 days. After corrosion testing, the samples were cleaned as per ASTM G1-03 [26] to remove the corrosion products. The aqueous

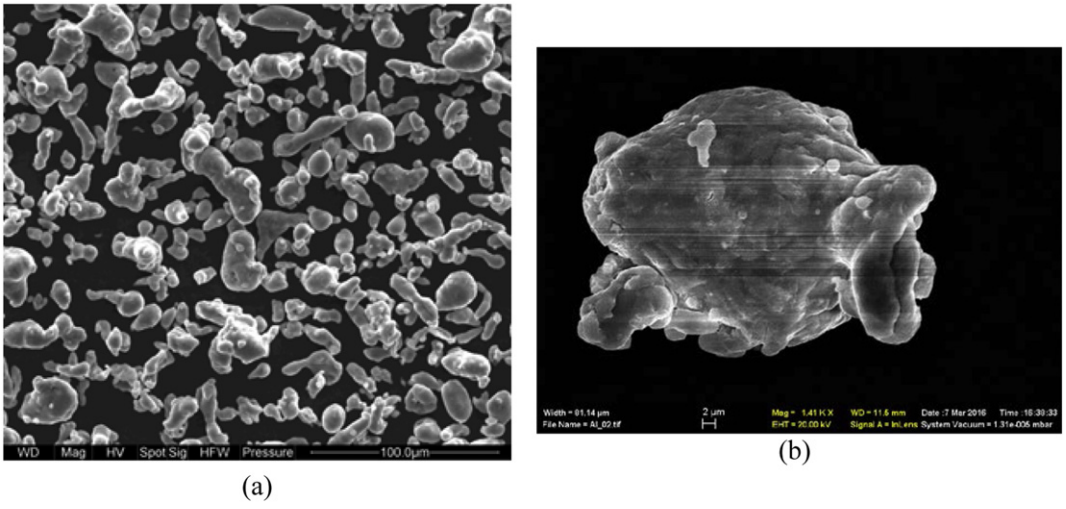


**Fig. 2.** SEM image of SST-A05011 feedstock powder showing (a) the irregular shape and distribution of the pure Al (Centerline Ltd.) (b) the shape and size of a typical particle, average particle size 20 µm.

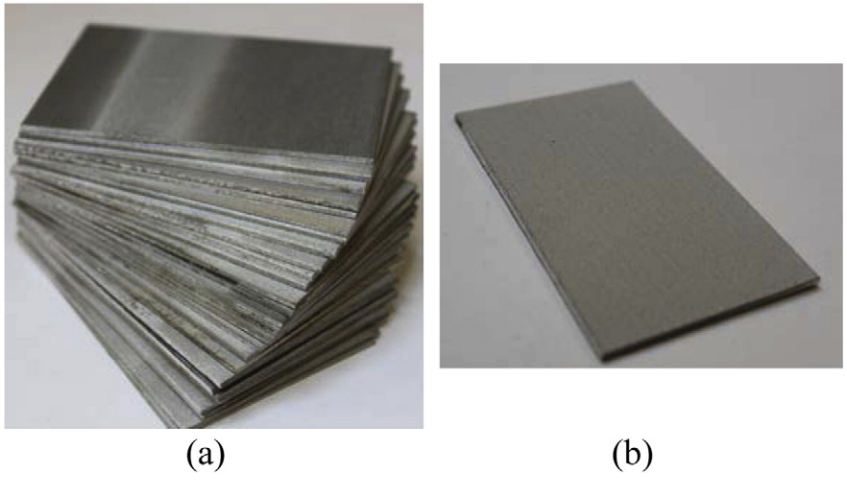


**Fig. 3.** (a) Bare and (b) Al cold spray coated coupons for corrosion testing.

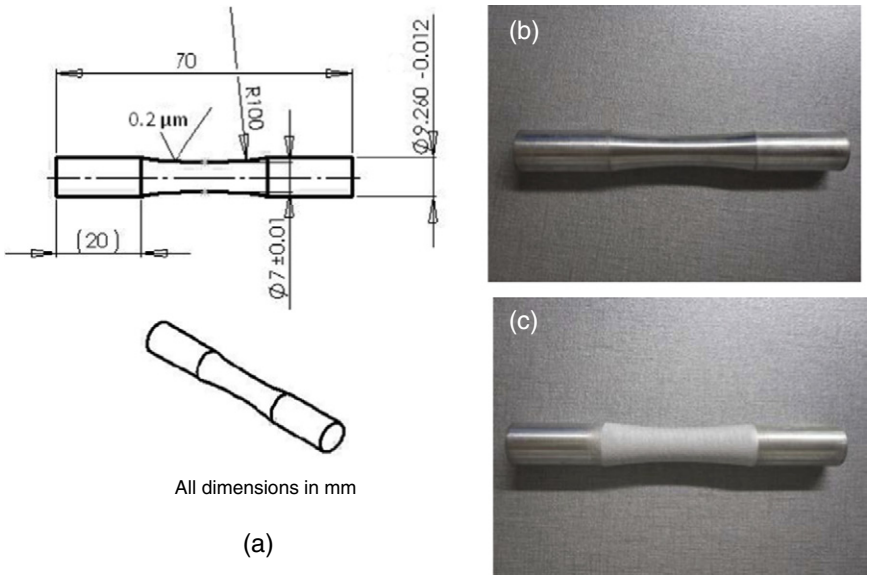


**Fig. 4.** Cylindrical specimens for fatigue testing in air and corrosive environment: (a) sample's dimensions and images of (b) bare and (c) Al cold spray coated specimens.


**Fig. 5.** The corrosion chamber (a) showing bulk and coated coupon distribution on racks before test, (b) edges of coated samples masked off by Miccrostop lacquer mask.

cleaning solution consisted of 200 g/l chromium trioxide ($CrO_3$), 10 g/l silver nitrate ($AgNO_3$), and 20 g/l barium nitrate ($Ba(NO_3)_2$). The samples were immersed in the solution for 1 min at a temperature of 20–25 °C, and then brushed lightly in reagent water to remove any loose products. In the case of heavy corrosion, the procedure for cleaning was repeated several times and factored in mass loss calculations as per ASTM G1-03.

A four-digit weighing scale was used for the weighing process before and after corrosion tests. A SJ-400 surface roughness tester was utilized to measure the surface roughness of the coated and uncoated coupons. Surface characterization and topographic analysis of the coupons were performed using an AltiSurf® 500 laser profilometer and Nanovea 3D imaging from which two and three-dimensional images were generated. These images enabled the surface characterization, measurement of functional parameters, pit measurements and 2D roughness analysis.

### 2.3. Fatigue and corrosion fatigue tests

Fatigue and corrosion fatigue tests were performed in an Instron rotating bending Moore machine (RBM). All tests were performed by controlling stress at constant amplitude, with the ratio of maximum to minimum stress equal to $-1$ ($R = -1$). The tests were performed at different stress amplitudes covering both low and high cycle fatigue. The maximum stress for the tests in air ranged from 100 MPa to 165 MPa. For the corrosion fatigue tests, maximum stress range was 40 MPa–120 MPa. A chamber was designed and retrofitted to the RBM to enable the corrosion fatigue test (Fig. 6). The chamber allowed flow

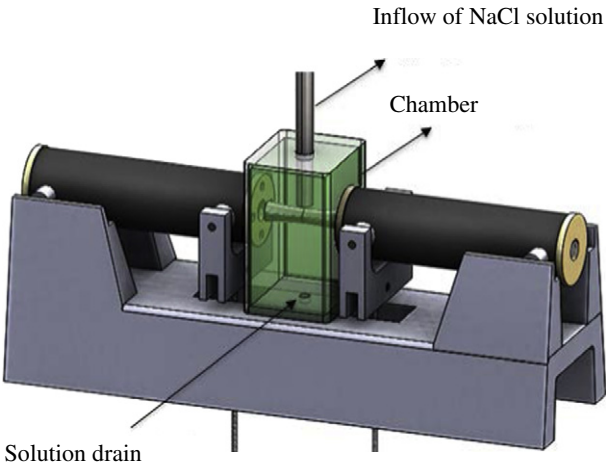


**Fig. 6.** Setup for the corrosion fatigue testing: rotating bending machine with the integrated corrosion chamber.

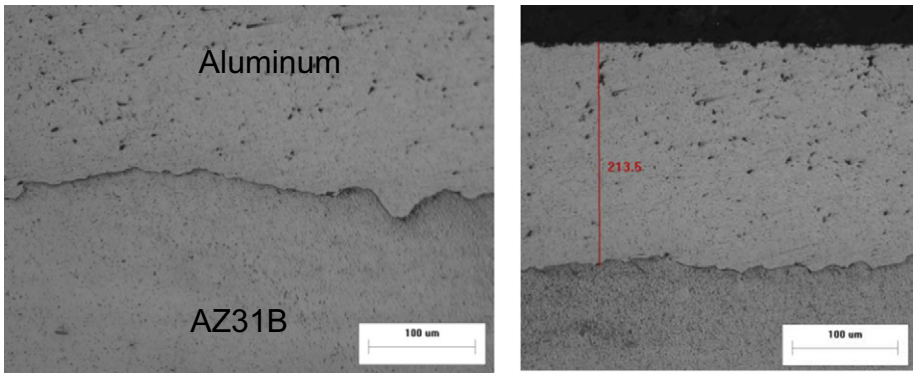


**Fig. 7.** Optical microscope images of the cross-section of pure Al coating on AZ31B substrate (a) showing a dense coating and a continuous bonding without any porosity, (b) sufficient and roughly uniform coating build-up with thickness in the range of 225 μm ± 25 μm.

of salt solution onto the specimen gauge surface at a constant rate during the fatigue testing. The salt solution flow into the chamber was facilitated through a tube from a large container with a capacity of 18.9 l of 3.5% NaCl solution, which had a controlling valve to control the solution flow rate. The rate was adjusted to 40 ml/min. This constant flow rate was enough to form a thin film of the NaCl solution on the specimen's gauge surface during the testing period. The solution that accumulated at the bottom of the pocket was drained and the salt solution tank was regularly filled with fresh NaCl solution. To prevent the galvanic corrosion of the specimen near the RBM bearing housing collets, a silicon resin was applied to the specimen's surface edges outside the gauge area. All corrosion fatigue experiments were performed at room temperature and at a frequency of 30 Hz.

## 3. Results and discussions

### 3.1. Coating quality

A cross-section of Mg substrate and Al coating interface/bonding is shown in Fig. 7. As it is evident from the image a good bonding with close to no porosity between the Mg substrate and the Al coating can be seen from the optical microscope image. This was expected as the pure aluminum particles go through severe plastic deformation due to their supersonic high impact kinetic energy creating a mechanical bond and forming low porosity with dense coating [20]. The coating was also showing a good build-up and had a final roughly uniform thickness in the range of 200 to 250 μm (Fig. 7b). The relative non-uniformity is attributed to several coating factors such as randomness of particle size, temperature and flow rate control resolution.

A total of fifteen sets of hardness measurements were performed on three different samples. The measurements included hardness of substrate (B), interface (I) and coating (C) as shown in Fig. 8 for the three areas. On average point B was 100 μm and point C was 120 μm from the interface. The results showed an average hardness reading (average ± one standard deviation) of 62.62 ± 1.35 HV for the substrate; 56.3 ± 0.61 HV for the interface; and 52.05 ± 1.42 HV for the coating. The hardness of the substrate (B) is larger than the average AZ31B extrusion hardness of 53 HV. This can be attributed to the work hardening effect near the surface of the substrate induced by the peening effect associated with the cold spray process. The high impact collision of particles with the surface of the substrate creates local plastic deformation on the surface and the particle [28]. The work hardening induced by such plastic deformation increases the hardness near the surface and close to the coating/substrate interface. Such increase in the hardness of the magnesium substrate was also reported by Bu et al. [20] and Xiong and Zhang [29] after being cold sprayed with pure aluminum. The hardness of pure aluminum close to the interface is also larger than its typical hardness of around 45 HV. The increase in hardness in pure aluminum may be related to the hammering effect of the new coating particles impacting the lower layers of coating. Similar findings were reported by other researchers [27,29].

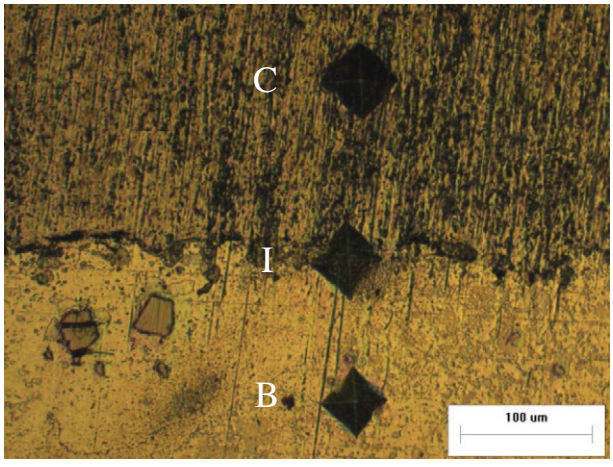


**Fig. 8.** Optical microscope image showing the hardness indentations at the three regions: base material (B), interface (I) and coat (C).

### 3.2. Corrosion tests

Bulk and Al cold spray coated AZ31B coupons were exposed to continuous salt fog environment per ASTM B117 for 33 cycles (days) with 3 samples extracted every 2 to 4 days. However, the test on coated samples was continued up to 90 days with lower extraction frequency. All samples were weighed before the test, after removing from the chamber, and after cleaning the corrosion product. The corrosion rate was calculated based on weight loss in mg/cm$^2$/day. Fig. 9 shows the bulk test samples after salt spray exposure over the 33 days of the tests. Visual observation showed that corrosion pits nucleated soon after the test started and showed a rapid growth up to cycles 4–6. The growth was somewhat slowed down afterwards and picked up again mid-way through the tests.

Fig. 10 shows the corrosion rate and percentage weight loss per number of corrosion cycles for the bulk magnesium. The trend of

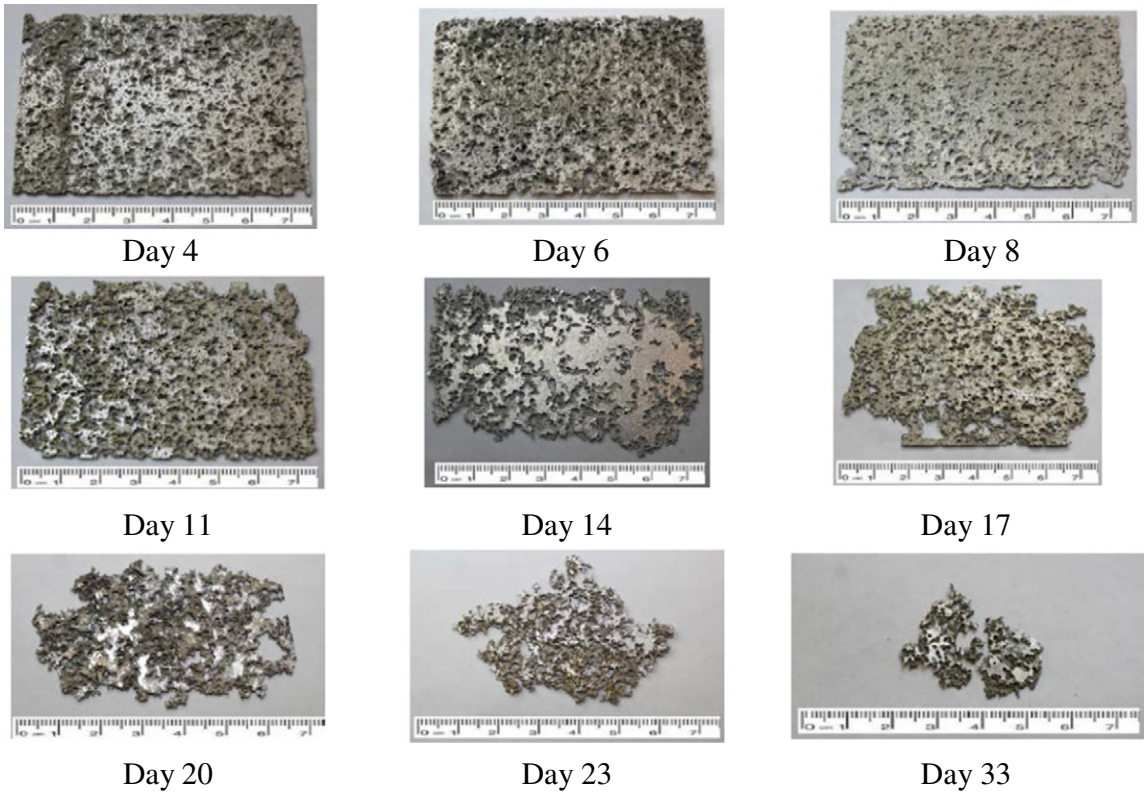


**Fig. 9.** Test samples after salt spray exposure over the 33-day period of the tests.

corrosion rate confirms the visual observation of rapid growth in first few cycles, decline until cycle 17 and growth thereafter. The same trend is followed by the average percentage weight loss as depicted by Fig. 10. These changes can be attributed to the formation of corrosion product on the surface of magnesium. Corrosion products consisting of mainly hydrated MgO and Brucite started to build up gradually and finally completely covered the surface of AZ31B around cycle number 4, which inhibited the aggressive electrolyte to reach to the fresh magnesium surface and impeded the pit growth. However, magnesium has a Pilling-Bedworth (P-B) ratio smaller than 1, which puts its surface oxide layer in tension and thus can result in a porous, cracked, non-protective oxide film. Moreover, the corrosion can be further accelerated when aggressive electrolyte species such as chloride are present. The

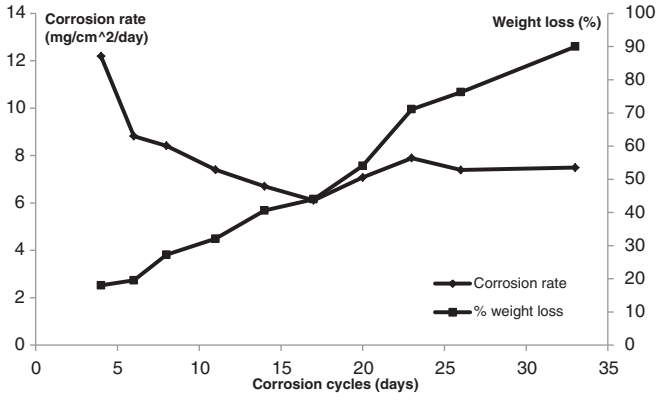


**Fig. 10.** Corrosion rate and average percentage weight loss of tested bulk AZ31B, AZ31B samples.

presence of chloride ions promotes the corrosion of the Mg alloy, generating hydrogen gas and magnesium chloride salt. The formation of soluble magnesium chloride weakened the protective $Mg(OH)_2$ film, resulting in exposure of fresh metal at sites where the protective scale is breached, and thereby, increases the corrosion rate [8,27]. The chloride ions that were trapped under corrosion products resulted in severe growth of pits through the depth resulting in loss of surface area as depicted in Fig. 9, images for day 17 onward, and Fig. 10.

Microstructural features such as grain size, secondary phases and their distribution, and abundant twinned microstructures may also promote the corrosion and pitting of magnesium alloys [7,9,29–32]. The grain boundaries and secondary phases can act as efficient cathodes to the Mg matrix in the alloy causing micro-galvanic corrosion [7]. The microstructure of as-received AZ31B extrusion was characterized on an etched [33] sample and the SEM image is shown in Fig. 11. The figure depicts the presence of the second phase in and around α-Mg grain boundaries, as well as many deformation twins. The size and distribution of the secondary phases are relatively uniform with average particle size of <5 μm. The volume fraction of the secondary phases is <5%.

Scanning Electron Microscope/Energy Dispersive X-ray (SEM/EDX) analysis for these secondary phases revealed the presence of Mg-Al-Mn (Fig. 11b) and Al–Mn (Fig. 11c) compounds. The presence of the second phases in the microstructure of Mg-Al alloys can have two effects on the corrosion behavior of the alloy depending on the volume fraction and the distribution of the second phases [7,9,34]. The second phase particles can act either as a barrier, or as a galvanic cathode to which the α-Mg is the galvanic anode. Unlike other magnesium alloys with higher content of Al, AZ31B did not show a strong β-phase presence, and the volume fraction of the second phase particle was very low with a relatively large distance between the particles which prevented formation of a continuous network of the second phase, and hence did not provide a corrosion barrier. On the other hand, the secondary phases and the grain boundaries can also act as galvanic

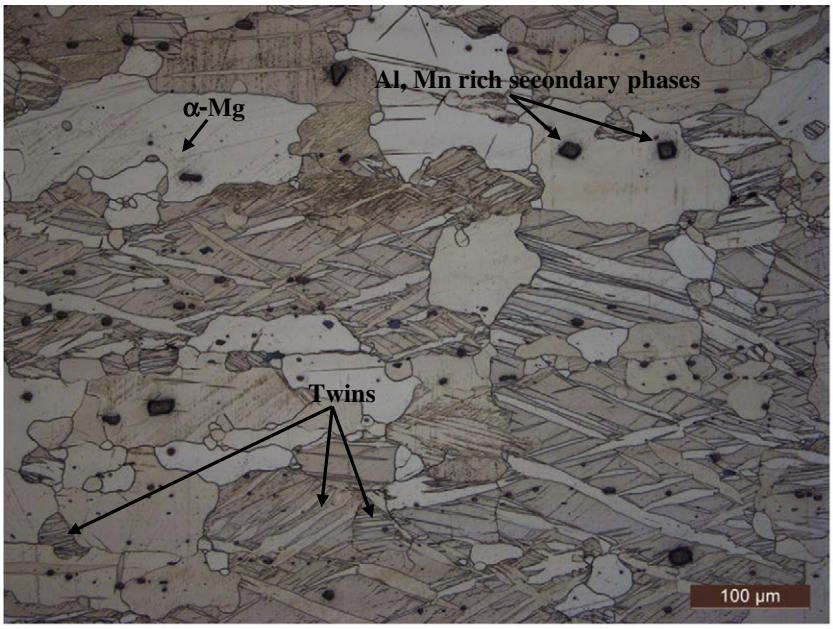


(a)

| Spectrum | Mg | Al | Mn |
|---|---|---|---|
| 1 | 69.90 | 13.03 | 17.07 |
| 2 | 63.25 | 20.31 | 16.44 |
| 3 | 40.71 | 34.49 | 24.80 |
| 4 | 49.73 | 32.26 | 18.01 |
| Max. | 69.90 | 34.49 | 24.80 |
| Min. | 40.71 | 13.03 | 16.44 |

All results in weight%

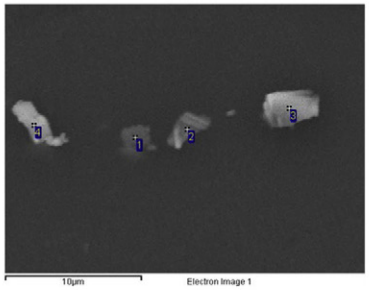


(b)

| Element | Weight% | Atomic% |
|---|---|---|
| Al | 22.60 | 37.29 |
| Mn | 77.40 | 62.71 |

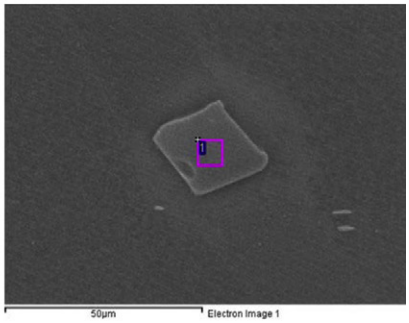


(c)

**Fig. 11.** (a) Optical cross section micrographs showing the microstructure of AZ31B and distribution of the second phase particles and twins; energy dispersive X-ray analysis of the detected secondary phases as (b) Mg-Al-Mn, and (c) Al-Mn.

cathodes to the α-Mg matrix. The Mn-rich compound exhibits a fairly high cathodic potential, and their cathodic potential can be 50–100 mV greater than the surrounding magnesium matrix [35]. The α-Mg grain size of AZ31B was large with the sparse second phase with large distance between them which contributed to the increase of the corrosion rate of the alloy [7,34]. In addition, the existence of twinned microstructures, as seen in Fig. 10a, could have also promoted the corrosion of the AZ31B [9].

*3.2.1. Al cold spray AZ31B coupons*

The testing duration for coated samples was extended to 90 cycles (days) with a longer time interval for sample removal. Fig. 12 shows the macrographs of the coated coupon surfaces after exposure to 5% salt spray over the duration of the test.

Visual examination of the tested coupons revealed that the Al cold spray coating has provided significant corrosion protection for the AZ31B substrate as compared to the bulk coupons. No corrosion pits were observed on the surface of any of the tested coupons. After 40 cycles of exposure, corrosion attack started to develop from the coupon edges where there was no cold spray coating (Fig. 12j, k, and l). Although the side edges of all coupons were masked off using the lacquer mask before corrosion testing, swelling due to moisture absorption allowed the salt solution to penetrate under the seal (Fig. 13a). As the exposure time increased the swelling increased, and in some cases

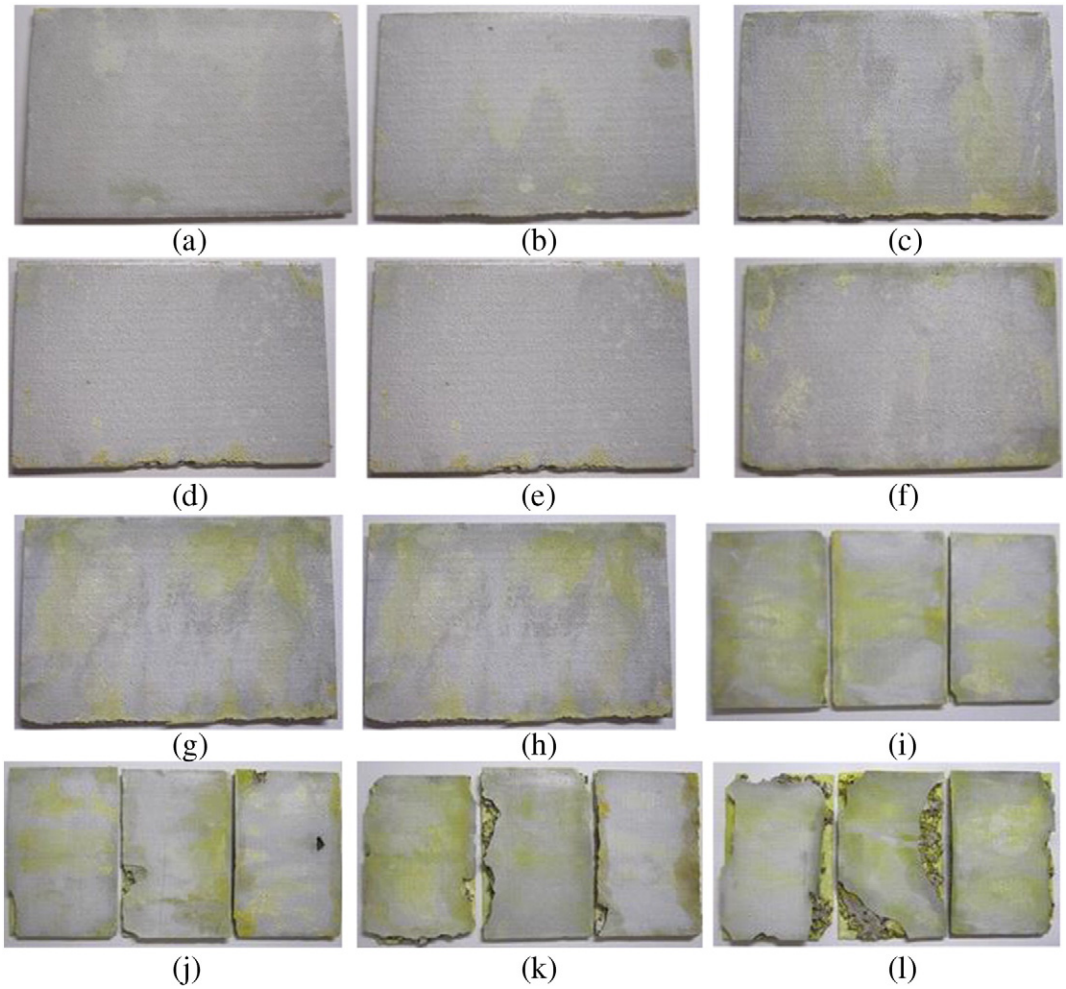


**Fig. 12.** Al-coated AZ31B coupons exposed to 5% salt spray after: (a) 4 cycles, (b) 8 cycles, (c) 11 cycles, (d) 14 cycles, (e) 17 cycles, (f) 20 cycles, (g) 23 cycles, (h) 26 cycles, (i) 33 cycles, (j) 40 cycles, (k) 60 cycles, (l) 90 cycles.

even resulted in mask being peeled off, allowing corrosion to proceed from the side (Fig. 13b). At 40, 60 and 90 cycles of testing, a large variation in the corrosion performance of the three replicate coupons was observed (Fig. 12j, k, and l) which may be attributed to challenges in masking uncoated areas. Similar challenges were reported in coating of magnesium substrates with a mixture of aluminum and alumina particles [16].

Fig. 14 shows the corrosion rate and percentage weight loss in coated samples. A slow corrosion rate increase up to cycle number 40 and then higher rate afterward are observed. Comparing to bulk samples, the corrosion rate declined by two orders of magnitude.

The surface roughness of each coated coupon was measured before and after the corrosion testing in order to examine the corrosion effect on the surface morphology. Fig. 15 shows a typical surface morphology

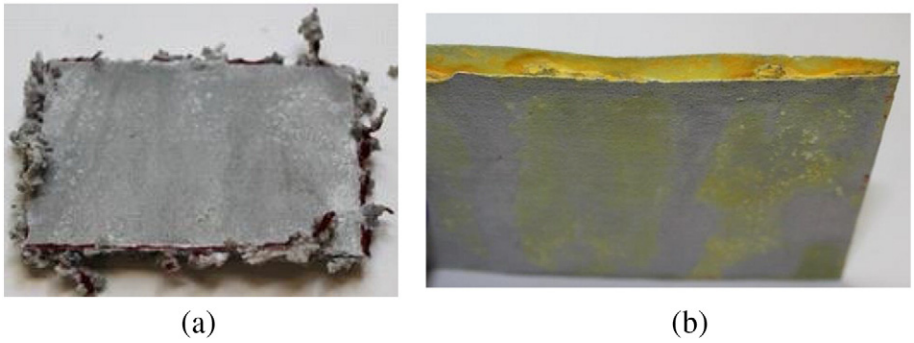


**Fig. 13.** (a) Swelling and peeling of the epoxy used for masking the edges, (b) a coated coupon after 40 days of testing showing the corrosion attack on Mg alloy substrate from the side edge while the Al coat remaining intact.

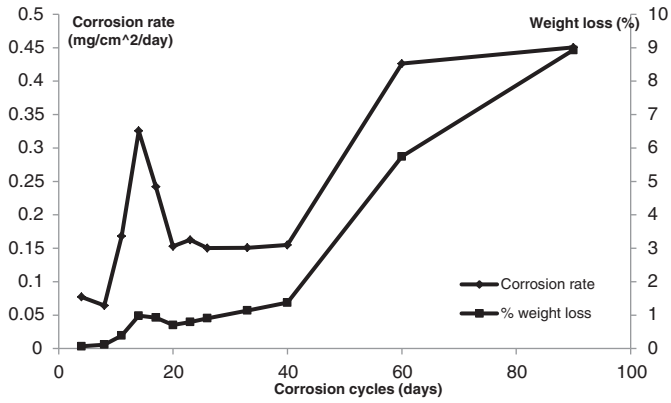


**Fig. 14.** Corrosion rate and average percentage weight loss of tested Al-coated AZ31B samples.

**Table 3**
Coated coupon surface roughness analysis.

| Cycle # (days) | # of tested coupons | Surface roughness average before testing (μm) | Surface roughness average after testing (μm) | Percentage change in surface roughness (%) |
|---|---|---|---|---|
| 4 | 1 | 150 | 215 | 43 |
| 8 | 1 | 183 | 288 | 57 |
| 11 | 1 | 146 | 259 | 77 |
| 14 | 1 | 165 | 300 | 82 |
| 17 | 1 | 133 | 221 | 66 |
| 20 | 1 | 187 | 250 | 33 |
| 23 | 1 | 176 | 269 | 52 |
| 26 | 1 | 144 | 204 | 42 |
| 33 | 3 | 172 | 351 | 104 |
| 40 | 3 | 170 | 398 | 134 |
| 60 | 3 | 154 | 462 | 200 |
| 90 | 3 | 163 | 702 | 331 |

measurement over an area of 70 mm × 45 mm with the root mean square average roughness values, and a 3D image for the scanned surface. The average roughness measurements for the coated coupons before and after the salt spray exposure are summarized in Table 3.

As shown in the table, the surface roughness for the Al cold spray coating before the corrosion testing ranged between 133 and 187 μm. This variation is due to the cold spray coating process with step over, standoff distance and variation of Al powder size. The change in the surface roughness before and after the corrosion testing up to cycle 26 was fairly steady and this was due to almost no variation on general surface and small variation at the edges because of protection quality. From cycle 33 up to the end of the test at cycle 90, the percentage change follows fairly linear trend. The large changes are due to the jagged edges and continuous detachment of the Al coating.

### 3.3. Corrosion fatigue

S-N curves of the coated and uncoated specimens tested in 3.5% NaCl solution are presented in Fig. 16.

For comparison purposes, and to provide a better understanding of the effect of the corrosive environment on the fatigue life of the AZ31B, the S-N curve from fatigue testing of AZ31B extrusion in air [36] is also shown in the same figure.

The fatigue life of coated AZ31B extrusion tested in air is improved when compared to the bulk AZ31B extrusion. This is attributed to the compressive residual stresses induced by cold spray coating [23,36]. The high impact velocity of aluminum particles on the magnesium substrate induces a local plastic deformation on the surface in the vicinity of impacted particle [28]. Spencer et al. [37] suggested that besides the dominant peening effect of cold spray, the thermal expansion coefficient mismatch between the Al coat and Mg substrate can also affect the formation and magnitude of the residual stress. In an earlier work, Shayegan et al. [23], using X-ray diffraction, measured the residual stress induced by coating pure aluminum on AZ31B substrate. They showed that the residual stress due to the impact of pure aluminum particles on stress-relieved AZ31B flat sample was in the range of −25 MPa at the substrate surface. The presence of compressive residual stress at the sample surface delays crack initiation and hinders its propagation which in turn enhances the fatigue life of AZ31B [28]. Similar increase in fatigue strength of AZ91D-T6 after cold spray coating with aluminum + alumina powder mixture was found by Xiong and Zhang [29]. However, they attributed this increase to the higher yield strength, work hardening at interface and higher bonding strength of the $Al/Al_2O_3$ and suggested that the residual stress plays a small role in fatigue enhancement of their coated samples. Since pure aluminum, with lower hardness than substrate is the coating powder in the present study, it is believed that the compressive stress induced by the coating process is the main cause of the slight fatigue strength increase when tested in air.

The fatigue strength of bulk and coated samples decreased under corrosive environment. Unlike the bulk and coated material cyclic behavior in air which shows a plateau in stress-life curve for lives over $3 \times 10^5$, there are no signs of sharp changes (plateau) in fatigue life under corrosive environment [38,39]. Therefore, no run-out test was possible for samples tested under corrosion fatigue. Fig. 17 shows the fracture surface of bulk AZ31B tested at 40 MPa in presence of 3.5%

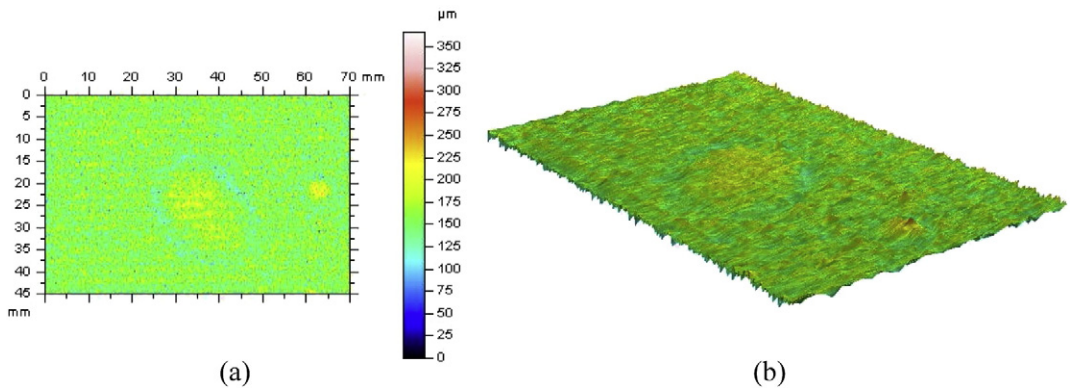


**Fig. 15.** Surface roughness analysis of coated AZ31B coupons performed by AltiSurf® 500 showing (a) roughness parameters and (b) surface 3D image.

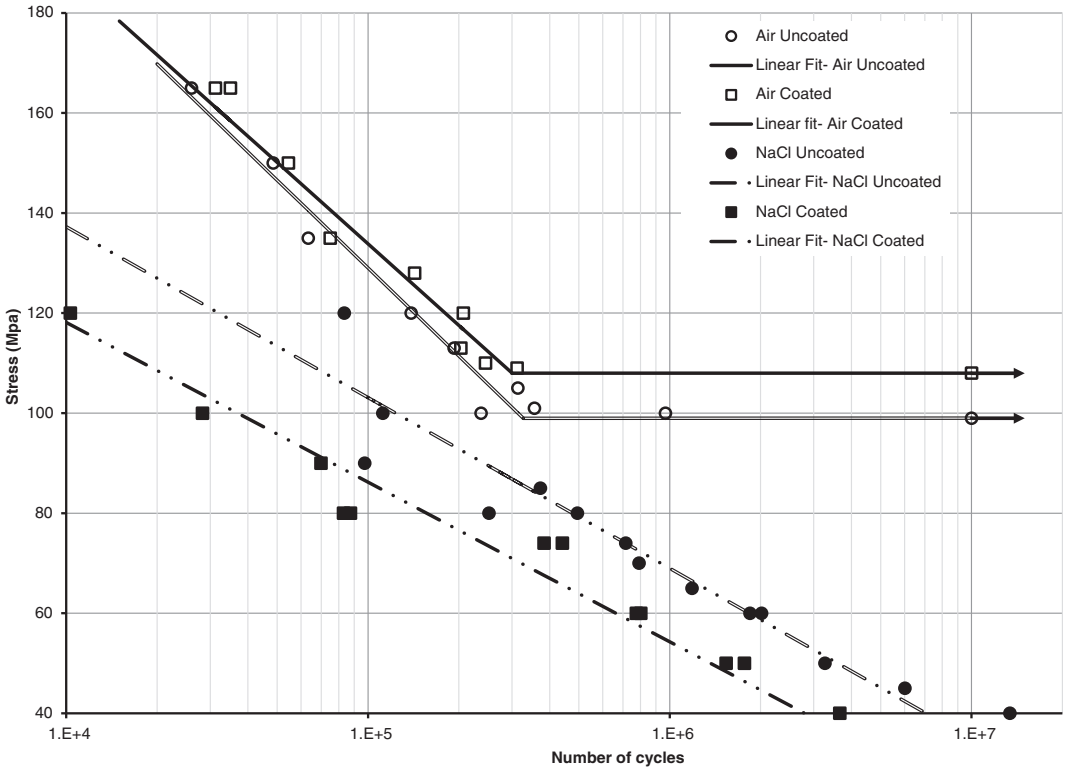


**Fig. 16.** S-N curves generated by the rotating bending test for coated and uncoated specimens in air and in 3.5% NaCl solution at 30 Hz frequency; all samples were machined in extrusion direction; data points with an arrow show run-out tests; test results in air are from [36].

NaCl solution that failed at $1.34 \times 10^7$ cycles. Large corrosion pits were traced all around the surface (red arrows in Fig. 17a). The thick yellow arrow points to an area where little corrosion pits coalesce after initial growth creating a large cavity. Multiple cracks emanating from surface corrosion pits growing toward the final fracture zone were traced (thin yellow arrows).

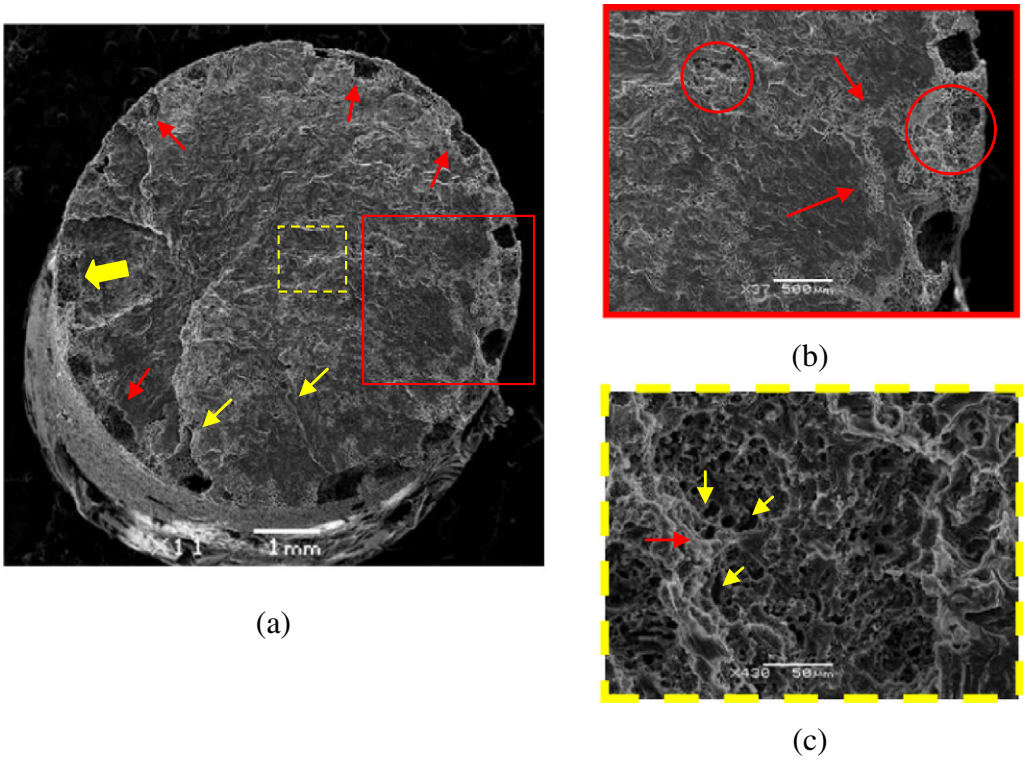


**Fig. 17.** Fracture surface of bulk AZ31B in corrosion fatigue test under stress amplitude of 40 MPa and failing after 5 days and 4 h exposure to 3.5% NaCl solution; (a) overall view, magnified images (b) near the surface and (c) of the final fracture zone.

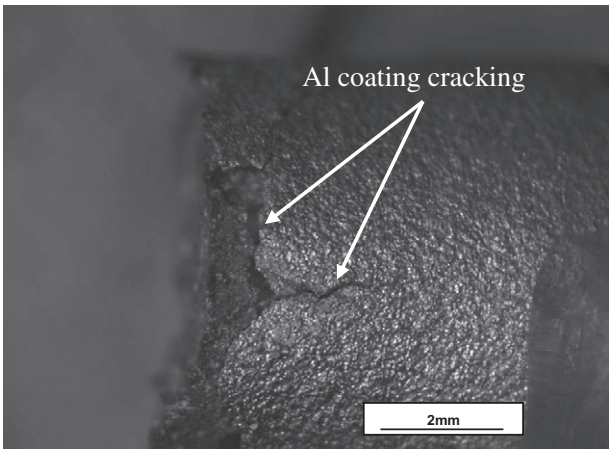


**Fig. 18.** Optical image of the surface cracking in Al cold spray coating on AZ31B.

Even though the stress level of the sample shown in Fig. 17 is very low, only about one third of compressive yield and one sixth of the tensile yield of bulk material, the mass loss and stress concentration due to pitting resulted in high-enough stresses to create cracks. As depicted by Fig. 10, bulk AZ31B corrosion rate has a sharp increase as soon as surrounded by NaCl solution (0–4 days), resulting in corrosion pitting at the surface. With the presence of stress, the pits act as a source of stress concentration and location of crack initiation. The solution then penetrates into the crack (Fig. 17b red arrows) creating further corrosion pits on the fracture surface (red circles in Fig. 17b) [39]. Fig. 17c shows the dimple-like final fracture zone. Besides the expected typical ductile fracture voids on fracture zone, corrosion product presence (red arrow) and corrosion pits nearby (yellow arrows) are also visible. Contrary to corrosion behavior of flat samples exposed to NaCl fog that shows corrosion products acted as a barrier for corrosion attacks hindering corrosion rate after 4 cycles (days), in corrosion fatigue the salt solution has found its way from the surface to the center of the specimen [39]. This is because of the stress concentration due to applied stress caused plastic deformation at the tip of the crack emanated from corrosion pits. The plastic zone and high stresses at crack tip ruptured the oxide and protective films formed on the surface of the crack, allowing fresh metal surface to be exposed to the electrolyte [38]. The combination of corrosive environment and stress is therefore accelerating the corrosion advancement, facilitating fracture at lower stress levels and expediting it at higher stress-levels.

In the corrosive environment (3.5% NaCl), the surface residual stress due to coating seemed to not help the fatigue life of the coated specimens, as the cold spray coated specimens showed a lower fatigue performance as compared with the uncoated specimens. Fig. 18 shows the optical image of the surface of a coated AZ31B coupon near the fracture surface after corrosion fatigue testing at a stress level of 88 MPa. An early crack on the Al coating is depicted in this figure. The SEM image of the fracture surface adjacent to this surface coating crack is shown in Fig. 19. It shows the cracking through the Al coating, corrosion pitting under the surface and local delamination from substrate.

The lower corrosion fatigue performance of coated samples as compared to bulk samples can be attributed to early breakdown of the pure aluminum coating due to its low ultimate tensile strength. The pure Al powder used in the cold spray process has a purity of 99.93% which has a lower ultimate tensile strength (~100 MPa) than AZ31B. With Al coating at the surface experiencing maximum stress in the rotating bending test, the mismatch in the mechanical properties between the Al coating and the AZ31B resulted in the failure, in the form of cracking, in the Al coating (rather than in the AZ31B substrate) at early stages of cyclic loading during the fatigue testing. The crack in coating formed a path for the electrolyte to penetrate and reach the fresh AZ31B substrate causing localized corrosion attack that led to the fast pit formation and growth under the coating. The localized galvanic corrosion, with the help of stress discontinuity between Al coating and Mg substrate because of their mechanical property mismatch, leads to local delamination of coating from substrate. Such delamination may also be related to fatigue crack propagation at interface of coating/substrate resulting from the differences in hardness between coating and substrate and plastic zone size at crack tip. The delamination advanced the corrosion pitting further than the initial localized pathway to the area of delamination (Fig. 19). Once these localized pits reached their critical size, crack on AZ31B initiated from the root of pits due to high level of stress concentration (Fig. 19). The crack propagation and further penetration of electrolyte through the crack path lead to final fracture.

Fig. 20 shows the fracture surface of coated sample tested at 80 MPa. SEM image of the final fracture zone is also shown in Fig. 20b. A mixed facet-type brittle as well as dimple-like ductile fracture can be traced in this figure. Trace of corrosion pits is also visible on the final fracture zone.

## 4. Conclusion

In this work, the corrosion and corrosion fatigue behavior of AZ31B cold spray coated with aluminum powder and uncoated coupons in NaCl environment were studied. The results were compared in order

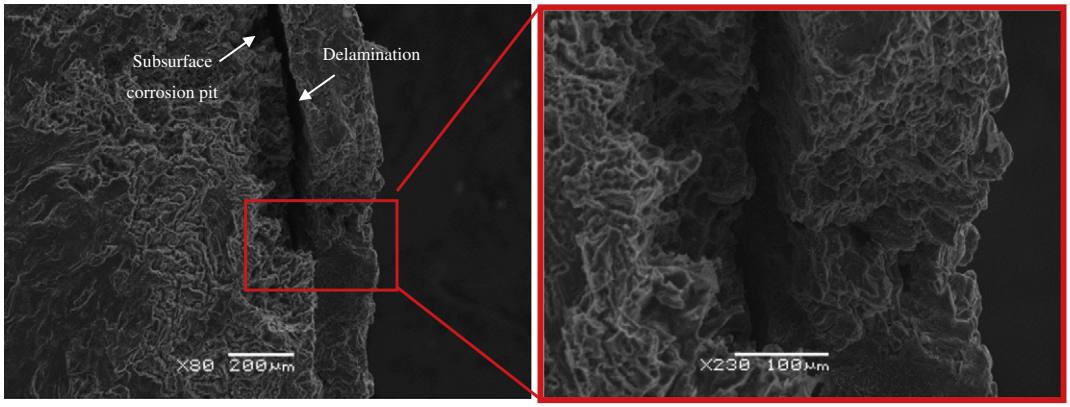


**Fig. 19.** SEM images of fracture surface of a coated sample showing magnified view of cracking of Al cold spray coating at a stress level of 80 MPa in the corrosion fatigue test, and showing corrosion cell between the coating and substrate.

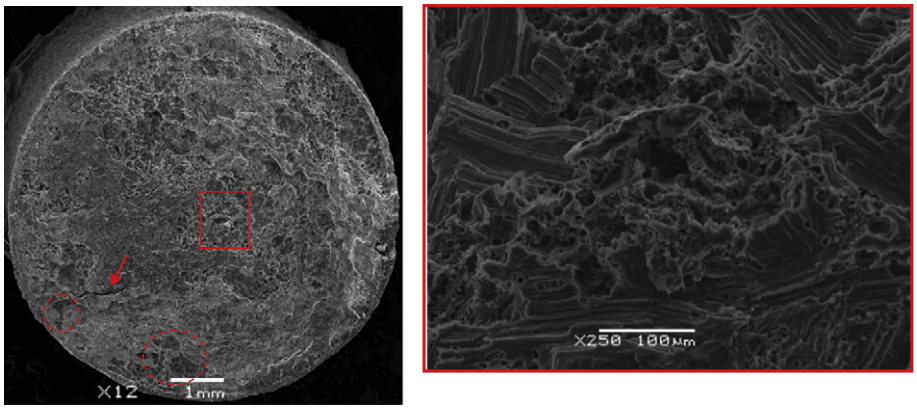


**Fig. 20.** Fracture surfaces of a coated AZ31B sample after the corrosion fatigue test at a stress of 80 MPa showing: (a) overall fracture surface, dashed circle showing under surface pitting and red arrow showing crack emanating from an undersurface pit; (b) mixed mode final fracture zone, showing cleavage-type brittle fracture with dimple-like ductile fracture coexisting together.

to ascertain the benefits of applying the Al cold spray coating to the corrosion resistance and corrosion fatigue properties of AZ31B alloy.

Based on the experimental results, the following conclusions can be drawn:

- The cold sprayed Al coating deposited on AZ31B alloy provided significant protection of the AZ31B from the corrosion attack. The strong adhesion and very low porosity of the Al coating are the main factors that resulted in the excellent corrosion performance of the coated AZ31B.
- Exposure to a corrosive environment (3.5% NaCl) significantly decreased the fatigue life of both the bare and coated samples of AZ31B extrusion as compared to their performance in air. Pitting, crack emanating from pits, and fracture of oxide layer at the tip of the crack due to plasticity surrounding the crack tip were the main fracture mechanisms.
- The low ultimate tensile strength of pure aluminum caused early cracking in the Al coating on the coated samples. These cracks, when tested in air, were arrested at the interface and did not cause early damage in the substrate. However, when tested in corrosive environment, the early crack acted as a pathway for corrosive solution to penetrate into the interface, causing localized corrosion and creating a stress concentration site. This led to early cracking on AZ31B substrate and hence poor fatigue performance of the coated sample.

## Acknowledgements

The first author would like to acknowledge the financial support of Saudi Basic Industries Corporation. Authors acknowledge the financial support from Natural Sciences and Engineering Research Council of Canada through Automotive Partnership Canada program under grant number APCPJ 459269-13. The efforts of Dr. Jianfeng Wang and Dr. Julio Villafuerte of Centerline, Windsor, Canada for coating of samples and scientific inputs are greatly appreciated. Technical support from Chao Shi and Jennifer Collier of CanmetMATERIALS, Natural Resources Canada; and Dr. Yuquan Ding, Rick Forgett, Neil Griffett and Richard Gordon of the University of Waterloo is acknowledged. The manuscript review and scientific inputs by Dr. Mark Kozdras of CanmetMATERIALS are gratefully acknowledged.

## References

[1] J.E. Gray, B. Luan, Protective coatings on magnesium and its alloys- a critical review, J. Alloys Compd. 336 (1) (2002) 88–113.
[2] M.S. Bhuiyan, Y. Mutoh, T. Murai, S. Iwakami, Corrosion fatigue behavior of extruded magnesium alloy AZ80-T5 in a 5% NaCl environment, Eng. Fract. Mech. 77 (10) (2010) 1567–1576.
[3] Y.L. Cheng, T.W. Qin, H.M. Wang, Z. Zhang, Comparison of corrosion behaviors of AZ31, AZ91, AM60 and ZK60 magnesium alloys, Trans. Nonferrous Metals Soc. China 19 (3) (2009) 517–524.
[4] Q. Qu, J. Ma, L. Wang, L. Li, W. Bai, Z. Ding, Corrosion behaviour of AZ31B magnesium alloy in NaCl solutions saturated with $CO_2$, Corros. Sci. 53 (4) (2011) 1186–1193.
[5] J. Liao, M. Hotta, N. Yamamoto, Corrosion behavior of fine-grained AZ31B magnesium alloy, Corros. Sci. 61 (2012) 208–214.
[6] B.A. Behrens, I. Schmidt, Improving the properties of forged magnesium parts by optimized process parameters, J. Mater. Process. Technol. 187 (2007) 761–765.
[7] G.L. Song, A. Atrens, Corrosion mechanisms of magnesium alloys, Adv. Eng. Mater. 1 (1) (1999) 11–33.
[8] H.J. Martin, M.F. Horstemeyer, P.T. Wang, Comparison of corrosion pitting under immersion and salt-spray environments on an as-cast AE44 magnesium alloy, Corros. Sci. 52 (11) (2010) 3624–3638.
[9] N.N. Aung, W. Zhou, Effect of grain size and twins on corrosion behaviour of AZ31B magnesium alloy, Corros. Sci. 52 (2) (2010) 589–594.
[10] T. Zhang, Z. Ji, S. Wu, Effect of extrusion ratio on mechanical and corrosion properties of AZ31B alloys prepared by a solid recycling process, Mater. Des. 32 (5) (2011) 2742–2748.
[11] X.B. Chen, N. Birbilis, T.B. Abbott, Review of corrosion-resistant conversion coatings for magnesium and its alloys, Corrosion 67 (3) (2011) (035005–1).
[12] P. Zhu, L. You Wang, G. Ren Qian, T. Hua Cao, M. Zhou, Copper coating electrodeposited directly onto AZ31 magnesium alloy, Anti-Corros. Methods Mater. 60 (3) (2013) 127–133.
[13] F. Chen, H. Zhou, B. Yao, Z. Qin, Q. Zhang, Corrosion resistance property of the ceramic coating obtained through microarc oxidation on the AZ31 magnesium alloy surfaces, Surf. Coat. Technol. 201 (9) (2007) 4905–4908.
[14] G.L. Song (Ed.), Corrosion Prevention of Magnesium Alloys, Elsevier, 2013.
[15] B.S. DeForce, T.J. Eden, J.K. Potter, Cold spray Al-5% Mg coatings for the corrosion protection of magnesium alloys, J. Therm. Spray Technol. 20 (6) (2011) 1352–1358.
[16] E. Irissou, J.G. Legoux, B. Arsenault, C. Moreau, Investigation of Al-$Al_2O_3$ cold spray coating formation and properties, J. Therm. Spray Technol. 16 (5–6) (2007) 661–668.
[17] K. Spencer, D.M. Fabijanic, M.X. Zhang, The use of Al–$Al_2O_3$ cold spray coatings to improve the surface properties of magnesium alloys, Surf. Coat. Technol. 204 (3) (2009) 336–344.
[18] Y. Tao, T. Xiong, C. Sun, H. Jin, H. Du, T. Li, Effect of α-$Al_2O_3$ on the properties of cold sprayed Al/α-$Al_2O_3$ composite coatings on AZ91D magnesium alloy, Appl. Surf. Sci. 256 (1) (2009) 261–266.
[19] Y. Tao, T. Xiong, C. Sun, L. Kong, X. Cui, T. Li, G.L. Song, Microstructure and corrosion performance of a cold sprayed aluminium coating on AZ91D magnesium alloy, Corros. Sci. 52 (10) (2010) 3191–3197.
[20] H. Bu, M. Yandouzi, C. Lu, D. MacDonald, B. Jodoin, Cold spray blended Al + $Mg_{17}Al_{12}$ coating for corrosion protection of AZ91D magnesium alloy, Surf. Coat. Technol. 207 (2012) 155–162.
[21] A. Eliezer, E.M. Gutman, E. Abramov, Y. Unigovski, Corrosion fatigue of die-cast and extruded magnesium alloys, J. Light. Met. 1 (3) (2001) 179–186.
[22] J. Albinmousa, H. Jahed, Multiaxial effects on LCF behaviour and fatigue failure of AZ31B magnesium extrusion, Int. J. Fatigue 67 (2014) 103–116.
[23] G. Shayegan, H. Mahmoudi, R. Ghelichi, J. Villafuerte, J. Wang, M. Guagliano, H. Jahed, Residual stress induced by cold spray coating of magnesium AZ31B extrusion, Mater. Des. 60 (2014) 72–84.
[24] ASM International Handbook, Volume 19: Fatigue and Fracture, ASM International, 1996.
[25] ASTM, B117, Standard Practice for Operating Salt Spray (Fog) Apparatus, 1997 ed. ASTM International, 1997.

[26] Standard, A. S. T. M. G1, Standard Practice for Preparing, Cleaning, and Evaluating Corrosion Test Specimens, ASTM International, West Conshohocken, PA, 2003 (2003, DOI: 10.1520/G0001-03).
[27] R. Ghelichi, D. MacDonald, S. Bagherifard, H. Jahed, M. Guagliano, B. Jodoin, Microstructure and fatigue behavior of cold spray coated Al5052, Acta Mater. 60 (19) (2012) 6555–6561.
[28] H. Jahed, R. Ghelichi, Residual stresses and fatigue life enhancement of cold spray, Modern Cold Spray, Springer International Publishing 2015, pp. 225–252.
[29] Y. Xiong, M.X. Zhang, The effect of cold sprayed coatings on the mechanical properties of AZ91D magnesium alloys, Surf. Coat. Technol. 253 (2014) 89–95.
[30] R.B. Alvarez, H.J. Martin, M.F. Horstemeyer, M.Q. Chandler, N. Williams, P.T. Wang, A. Ruiz, Corrosion relationships as a function of time and surface roughness on a structural AE44 magnesium alloy, Corros. Sci. 52 (5) (2010) 1635–1648.
[31] J.D. Majumdar, R. Galun, B.L. Mordike, I. Manna, Effect of laser surface melting on corrosion and wear resistance of a commercial magnesium alloy, Mater. Sci. Eng. A 361 (1) (2003) 119–129.
[32] M.G. Fontana, Corrosion principles, Corrosion Engineering, McGraw-Hill, Boston 1986, pp. 12–38.
[33] M.M. Avedesian, H. Baker (Eds.), ASM Specialty Handbook: Magnesium and Magnesium Alloys, ASM international, 1999.
[34] G. Song, A. Atrens, M. Dargusch, Influence of microstructure on the corrosion of diecast AZ91D, Corros. Sci. 41 (2) (1998) 249–273.
[35] M.C. Merino, A. Pardo, R. Arrabal, S. Merino, P. Casajús, M. Mohedano, Influence of chloride ion concentration and temperature on the corrosion of Mg–Al alloys in salt fog, Corros. Sci. 52 (5) (2010) 1696–1704.
[36] E. Kalatehmollaei, H. Mahmoudi-Asl, H. Jahed, An asymmetric elastic–plastic analysis of the load-controlled rotating bending test and its application in the fatigue life estimation of wrought magnesium AZ31B, Int. J. Fatigue 64 (2014) 33–41.
[37] K. Spencer, V. Luzin, N. Matthews, M.X. Zhang, Residual stresses in cold spray Al coatings: the effect of alloying and of process parameters, Surf. Coat. Technol. 206 (19) (2012) 4249–4255.
[38] Z.Y. Nan, S. Ishihara, T. Goshima, Corrosion fatigue behavior of extruded magnesium alloy AZ31 in sodium chloride solution, Int. J. Fatigue 30 (7) (2008) 1181–1188.
[39] Y. Unigovski, A. Eliezer, E. Abramov, Y. Snir, E.M. Gutman, Corrosion fatigue of extruded magnesium alloys, Mater. Sci. Eng. A 360 (1) (2003) 132–139.